International Journal of Infrared and Millimeter Waves, Vol. 5, No. 2, 1984

THE ATMOSPHERIC WATER VAPOR CONTINUUM BELOW 300 GHz*

Hans J. Liebe

Institute for Telecommunication Sciences
National Telecommunications and Information Administration
U. S. Department of Commerce
Boulder, Colorado 80303

Received October 31, 1983

Absolute attenuation rates due to water vapor and moist nitrogen have been measured in the laboratory at 138 GHz, 282 and 300 K, pressures up to 1.5 atm, and relative humidities from 80 to 100 percent. The computer-controlled measuring system is comprised of a millimeter wave resonance spectrometer (0.15 km effective path length) and a humidity simulator. Several shortcomings of earlier measurement attempts have been rectified. The data are interpreted as a water vapor continuum spectrum consisting of two terms, namely strong self-broadening (H_2O-H_2O) plus foreign-gas-broadening (H_2O-N_2) contributions. Implications of the new results for modeling atmospheric EHF window transparencies and for revising established H_2O line broadening theory are discussed.

Key Words: Atmospheric radio wave propagation; high-humidity spectrometer; millimeter wavelength region; water vapor continuum absorption

*The work was supported in part by the U.S. Army Research Office under Contract ARO 101-83.

0195-9271/84/0200-0207$03.50/0

Introduction

Millimeter wave propagation through the atmosphere is affected by meteorological phenomena such as humidity, fog, clouds, and precipitation. System applications require a detailed knowledge of atmospheric propagation limitations and their dependency upon relevant meteorological parameters. The influence of the intervening atmosphere upon radio waves can be quantified by a propagation model. In clear air, water vapor and oxygen absorption cause frequency-dependent signal attenuation, propagation delay, ray bending, and medium noise. Prediction of these propagation effects is accomplished by a broadband model of the complex refractivity N (1). To cover frequencies up to 300 GHz, a reliable expression for N requires more than 200 coefficients. The refractivity N is formulated in units of parts per million (ppm) and consists of three components

$$N = N_o + D(f) + jN''(f) \qquad \text{ppm}$$

where N_o is the frequency independent refractivity, and $D(f)$ and $N''(f)$ are frequency-dependent dispersion and absorption terms arising from the molecular spectra of H_2O and O_2.

The specific rates of the propagation medium are power attenuation

$$\alpha = 0.1820fN''(f) \quad \text{dB/km} \tag{1}$$

and delay

$$\beta = 3.336[N_o + D(f)] \quad \text{ps/km} , \tag{2}$$

where the frequency f is in units of GHz.

This paper addresses millimeter-wave water vapor attenuation rates. There has been a long-standing discrepancy between theoretical spectroscopic predictions and experimental data obtained from both laboratory and field measurements (3,4). Marked differences occur in the window ranges located around 35, 90, 140, and 220 GHz (2), where experimental attenuation exceeds the theoretical values. Since excess factors between 2 and 5 are involved, it has been speculated that unidentified absorbers related to H_2O

(dimers, clusters, etc.) might be involved. Results for α from controlled laboratory experiments in the 140 GHz window are reported which help to clarify the water vapor excess problem.

Water Vapor Millimeter Wave Spectroscopy

Water in both vapor and liquid states obscures the millimeter wave transparency of the troposphere. Frequency dependence and magnitude of H_2O attenuation are both distinctly different for the same (1 mm) absorber thickness in water, rain, suspended droplet, moist air, and pure water vapor form, as illustrated in Figure 1 (2).

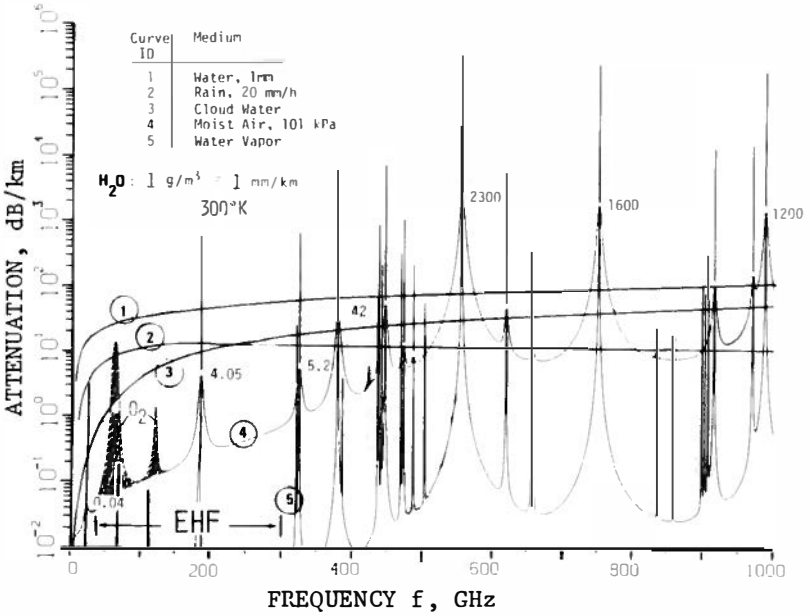

Figure 1. Normalized specific H_2O attenuation over the frequency range 5 to 1000 GHz for five phase states: water ①, rain ②, suspended hydrometeors ③, moist air ④, (numbers shown indicate selected H_2O attenuation peaks), and pure water vapor ⑤.

Water vapor attenuation α_w depends on absolute humidity

$$v = 7.219e\theta \quad g/m^3 \tag{3}$$

where e is the partial vapor pressure in kPa = 10 mb and $\theta = 300/T$ is a relative inverse temperature indicator. Water vapor pressure e is limited by relative humidity

$$RH = 41.51e\theta^{-5}10^{(9.834\theta-10)} \leq 100\% . \tag{4}$$

The attenuation α_w has its origin in the absorption lines of water vapor. In principle, α_w can be evaluated from a line-by-line summation of all line features, each contributing at a given frequency as prescribed by a line shape function F(f). Six reported H_2O line data bases (LB) are indexed in Table I.

Table I. Available data bases for H_2O absorption lines

ID	Frequency cutoff	Number of lines (n)	Remark	Ref.
	THz			
LB1	537	38350	AFGL Tape	5
LB2	126	17201	French version	6
LB3	30	2277	Rotational Spectr.	7
LB4	3	151	Radio Astronomy	8
LB5	1	30(+α_c)	EHF approximation	1
LB6	1.1	17	Russian version	18

The extreme low frequency wings of about 180 stronger (i.e., at ν_o more than 10^5 times the value of α_w at 100 GHz) lines below 12 THz make contributions in the EHF range. Six different standard line shape functions F(f) are available to assess these contributions. Usually, the shape functions are governed by two spectroscopic parameters: line center frequency ν_o and width γ. Recently a third parameter, the population "frequency",

$$\nu_B = 2kT/hc = 12510/\theta \quad GHz, \tag{5}$$

has been introduced (4b, 4h). When these shape functions are normalized to unity at the center ν_o, the functional dependences given in Table II are obtained.

Table II. Normalized pressure-broadened line shape functions

Normalization: $\alpha_w = \alpha_o(\nu_o)F(z)$ for a single line,

$a = \gamma/\nu_o$, $b = \nu_o/\nu_B$, $z = f/\nu_o$

ID*	F(z)	$\delta\times10^3$ (Eq.7)
SL	$a^2z\ [a^2+(1-z)^2]^{-1}$	1.9
FL	$a^2z\ \{[a^2+(1-z)^2]^{-1} - [a^2+(1-z)^2]^{-1}\}$	-0.001
GR	$a^2z^2\ [a^2z^2+(1-z^2)^2/4]^{-1} \simeq$ (FL)	-0.001
VW	$a^2z^2\{[a^2+(1-z)^2]^{-1} + [a^2+(1+z)^2]^{-1}\}$	637
MGR	(GR)z	8.2
MVW	(VW)[tanh(bz)/tanh b]/z	16.6

*SL = short Lorentzian, FL = full Lorentzian, GR = Gross, VW = Van Vleck-Weisskopf, MGR = modified GR, MVW = modified VW (10).

The intensity distribution of a strong H_2O line was traced with the shape functions listed in Table II and the example is exhibited in Figure 2. Within the line core, that is $F(z) \geq 10^{-4}$ or $z \simeq 0.8$ to 1.2, all shapes are alike and it is inconsequential which one is used. On the other hand, far-wing intensities depend very much on the chosen frequency distribution function. For example, the relative contribution of the line shown in Figure 2 can vary at 100 GHz over a range 1(MGR):75(SL).

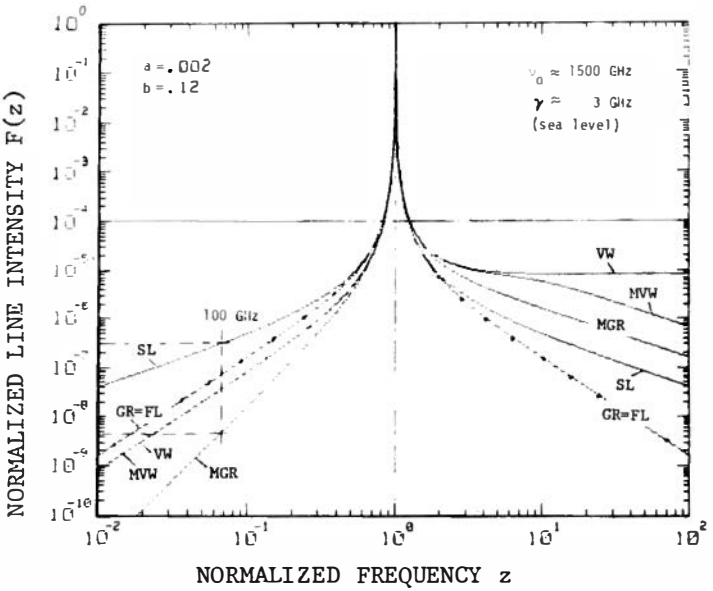

Figure 2. Normalized pressure-broadened line shapes F(z) (see Table II) applied to a single H_2O line. The line is actually centered at ν_o = 1669.907 GHz with a peak attenuation rate $\alpha_o = 2.3 \times 10^5$ dB/km in sea level air (θ = 1, v = 10 g/m^3).

The EHF (30 to 300 GHz) propagation model developed by us (1) uses for reasons of computational economy 30 local H_2O lines below 1 THz (LB5, Table I). A theoretical assessment of EHF attenuation $\alpha_w = \alpha_\ell + \alpha_c$ was accomplished on the basis of LB3 by subtracting the line contributions below 1 THz from all 2277. The far-wing contributions from pressure-broadened lines above 1 THz are then fitted below 300 GHz to a water vapor continuum absorption

$$\alpha_c = k(p/101)v^x\theta^y(f/100)^u \quad \text{dB/km}, \qquad (6)$$

where p is dry air pressure in kPa. One recognizes exponents for vapor concentration (x), temperature (y), and frequency (u) dependences. Applying various shape functions (Table II) to LB3 led to the results summarized in Table III. As expected, the scale factor k varies over a wide range. Also, one notices that all three exponents are influenced by the selected shape function.

Table III. Theoretical EHF water vapor continuum coefficients (Eq.6)

Line Shape	k	x(v)	y(T)	u(f)
MGR	0.0014	1.00	2.0	2.5
MVW,VW	0.0064	1.01	1.4	2.1
GR,FL	0.012	1.02	1.4	2.0
SL	0.064	1.05	1.2	1.2

The functions were tested for finite integrated (f = 0 to ∞) line absorption to decide which shape is most plausible. A limited-range numerical integration resulted in residuals,

$$\delta = (1/\pi a)\int_{0.001}^{1000} F(z)dz - 1, \qquad (7)$$

and it follows (see Table II) that some deviate considerably from the ideal $\delta = 0$. Based on Eq.(7), the shapes VW, MVW and MGR can not be considered valid intensity descriptors of a pressure-broadened line over a wide frequency range (22)--and the others are probably overtaxed by expecting them to predict eight significant orders of attenuation rate.

Water Vapor Continuum Absorption

The attenuation rate α due to a single line is calculated with Eq.(1), where the product of strength S and shape F defines

$$N''(f) = SF(f) \quad \text{ppm} \ . \qquad (8)$$

The line properties are formulated in Ref.(1) at $\Theta = 1$ (300 K) by a set of spectroscopic coefficients b_1 to b_3. In the low frequency far wing ($\gamma << f << \nu_o$), any of the theoretical line shapes in Table II is proportional to the width γ; however, individual continuum shape approximations $F_c(f \to 0) =$

$$4f^2\gamma/\nu_o^4 \ \text{[MGR]}, \quad 2f\gamma/\nu_o^3 \ \text{[MVW,VW]}, \qquad (9)$$

$$4f\gamma/\nu_o^3 \ \text{[GR,FL]}, \quad \gamma/\nu_o^2 \ \text{[SL]},$$

predict successively higher contributions (see Fig. 2, Table III).

Strength S and width γ of a typical single H_2O line, pressure-broadened by a mixture of water vapor (e) and dry air (p), are given by

$$S \simeq b_1 e \theta^{1.5} \quad \text{kHz} \tag{10}$$

and

$$\gamma \simeq b_3 (m \cdot e + p) \theta \quad \text{GHz} \quad . \tag{11}$$

Water vapor continuum attenuation α_c due to n H_2O absorption lines described by FL or GR shapes can be approximated with Eqs.(1), (8) to (11) in the form

$$\alpha_c \simeq 0.73 f^2 e (m \cdot e + p) \theta^{2.5} \times \sum_{i=1}^{n} (b_1 b_3 / \nu_o^3)_i \quad . \tag{12}$$

The continuum spectrum consists of a self-broadening term ($\propto e^2$) and a foreign-gas-broadening term ($\propto ep$),

$$\alpha_c = (k_s e^2 + k_f e p) \theta^y \quad \text{dB/km} \quad , \tag{13}$$

where line shape theory predicts the coefficients

$$k_s = 3.5 f^2 \sum_{i=1}^{n} (b_1 b_3 / \nu_o^3)_i = m k_f \tag{14}$$

and the exponent

$$y = 2.5 \quad . \tag{15}$$

The ratio

$$m = k_s / k_f = 4.80 \tag{16}$$

is the pressure-broadening efficiency of pure water vapor with reference to dry air, determined by measurements in line cores (15). There is ample evidence (4a, 10, 12) that in the EHF range, besides local lines, the low frequency wing of the self-broadened rotational H_2O spectrum centered around 9 THz is much stronger than predicted by Eq. (12). A careful review of H_2O continuum absorption by Burch (10), including all of his reported data, uncovered increases of the broadening efficiency in the far wings of lines ranging between $m \simeq 20$ at 300 GHz and $m \simeq 50$ at 30 GHz (see later, Table IV).

The laboratory experiment described in the next section was prepared to measure absolute attenuation rates α at three EHF window frequencies (i.e., 92, 138, and 220 GHz) under conditions reaching water vapor saturation. Absorption by neighboring lines is small, so that to first order $\alpha \simeq \alpha_c$. Attenuation data are expected to behave as predicted by Eq.(13). The ongoing experimental studies are aimed at securing accurate coefficients k_s, k_f, and y, as well as looking for possible anomalies not supported by the pressure-broadened rotational spectrum of the H_2O molecule. The last section of this paper presents first attenuation results obtained at 138 GHz and discusses their implications to EHF propagation modeling.

Millimeter Wave Spectrometer for High Humidity Studies

Controlled experiments that simulate atmospheric conditions provide test cases for studying specific contributions to N in isolation. Assessments of basic physical principles underlying the attenuation rate α are difficult to make from measurements in the actual atmosphere. Reliability, precision, and scale of supporting meteorological data compromise the quality of most field observations. The expected EHF window attenuation is low in a spectroscopic sense (<10 dB/km) and requires long path lengths (>100 m) for a reliable detection. A semi-confocal Fabry-Pérot resonator with a high Q value (437,000 at 138 GHz) offered a good compromise between compactness and detection sensitivity. The computer-controlled measuring system consists of the millimeter wave resonance spectrometer and a humidity simulator. An insulated box contains a high-vacuum stainless steel vessel which houses a temperature-controlled mini-lake (10 cm across) and the radio test path (see Figure 3). Signals at frequencies between 30 and 300 GHz can be employed over equivalent free-space path lengths between 500 and 50 m; temperatures are controlled to better than 1/100 of a degree Celsius; pressure ranges over seven orders of magnitude (10^2 to 10^{-5} kPa); and relative humidity is varied between 0 and 100 percent.

Schematical diagrams of physical (Figure 3) and electronic (Figure 4) arrangements convey an overview of the experiment. Quasi-static diffusion mixing was chosen to generate well defined humidities inside the spectrometer cell. A temperature controlled water reservoir serves as

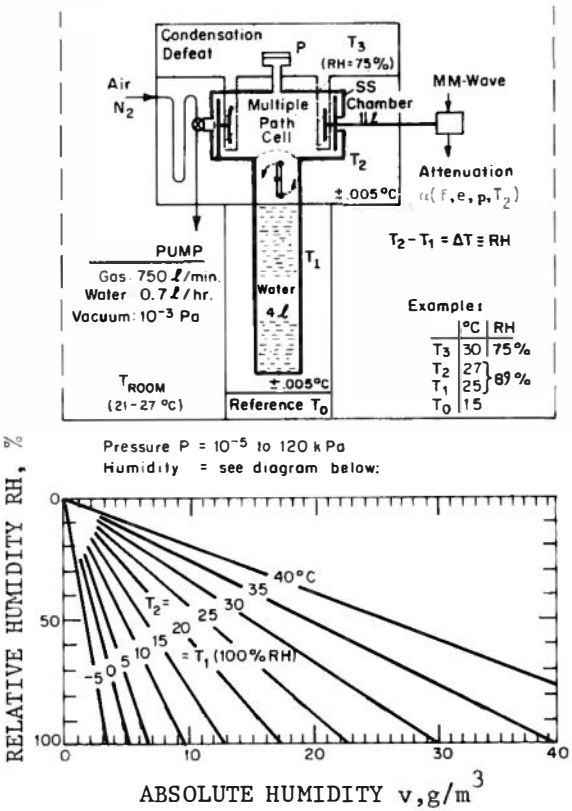

Figure 3. Cross-section of millimeter wave resonance spectrometer and built-in humidity generator. Note three different, extremely stable temperature zones, $T_1(\Theta_1)$ to $T_3(\Theta_3)$. Relative humidity inside the cell is (Eq. 4): log (RH) = $2\text{-}9.834\ (\Theta_1 - \Theta_2) + 5\ (\log\Theta_1 - \log\Theta_2)$ %. Absolute humidity v is shown in the diagram.

the vapor source. Electropolished stainless steel was used exclusively as construction material. Various hydrophobic coatings were studied as possible means for neutralizing the absorption/desorption cycle on surfaces exposed to water vapor (4d), but were abandoned in favor of slightly heating the mirrors. Four fast-responding (τ < 1s) temperature sensors inside the cell diagnose any disturbance of the gas equilibrium. Data acquisition is computer-controlled.

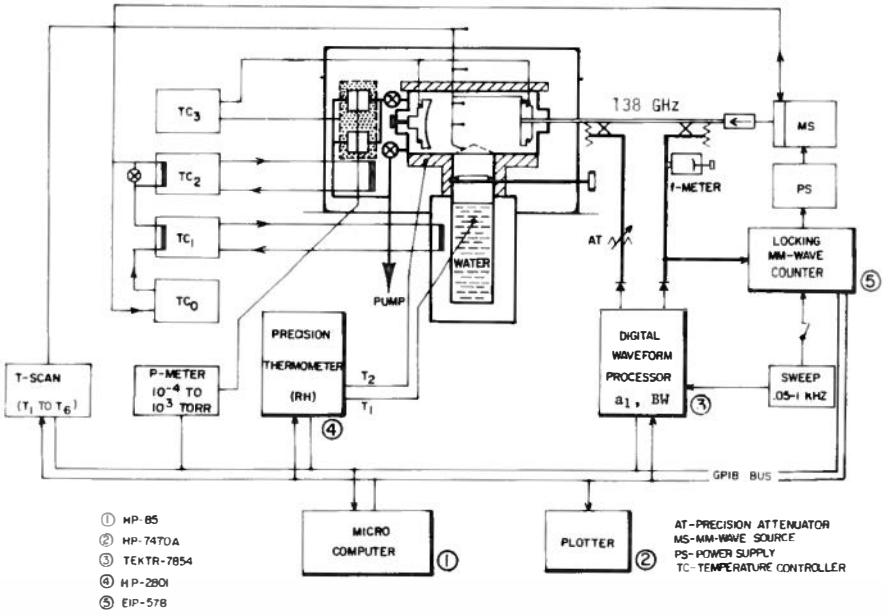

Figure 4. Schematic of high-humidity millimeter wave spectrometer and computer-controlled data acquisition system.

User-friendly software allows the choice of several modes of continuous operation over time scales from one minute to many days. The resonance signal that carries the absorption information is detected with a digital waveform analyzer. The analyzer performs the following tasks under computer control: averaging (1 to 100×), baseline normalization, peak value (P-P) and bandwidth (BW) measurements.

Detection Principles

The dimensionless complex refractivity N is a macroscopic measure of the interaction between gas molecules and mm-waves. Real and imaginary parts are related by the Kramers-Kronig formula. The response curve of a gas-filled resonator is

$$a(f) \propto \{Q^{-1} + Q_M^{-1} + j2[(f/f_R)(1 + N'\times 10^{-6}) - 1]\}^{-1}, \quad (17)$$

where Q is the loaded Q-value, f_R is the resonance frequency of the evacuated resonator, and a Q-value of the gas is defined by

$$Q_M = 91021 \times f_R/\alpha = 10^6/2N'' \quad . \tag{18}$$

Two modes of spectrometer operation follow from Eq.(17) when the evacuated resonator is slowly subjected to a gas pressure P:

Absorption mode. The resonator is swept periodically across its resonance f_R in order to measure α. The shape of the response curve, Eq.(17), appears as a pulse series a(t) when rectified with the detection law β. The decrease in the maximum amplitude $a_o(P = 0)$ at f_R to values $a_1(P)$ is sensed by a peak detector. The attenuation rate is obtained from

$$\alpha = 4.343[(a_o/a_1)^{1/\beta} - 1]/L_R \quad \text{dB/km} \quad , \tag{19}$$

where the effective path length is given by

$$L_R = 4.771 \times 10^{-5} Q/f_R \quad \text{km} \quad . \tag{20}$$

From a(t), the peak detector records an absorption pressure profile

$$a_1(P) = a_o/\{[\alpha(P)L_R/4.343] + 1\}^{\beta} \quad , \tag{21}$$

where the total pressure P = e + p is measured and the expected attenuation rate α is predicted by Eq.(13). A digital waveform processor (see Figure 4) resolves amplitude changes to about 0.1 percent, allowing a detection sensitivity of (16)

$$\alpha_{min} \geq 92 f_R/Q$$

(e.g., F_R = 138 GHz, Q = 437000, $\alpha_{min} \simeq$ 0.05 dB/km). (22)

Refraction mode. To measure N', the shift in resonance frequency by a small amount to f_N is tracked and refraction is given by

$$N' = 10^6[f_R - f_N(P)]/f_R \quad \text{ppm.} \tag{23}$$

Frequency changes of f_R can be compensated with the tuning micrometer, allowing a resolution of $N'_{min} \simeq$ 0.6 ppm.

Specifications for the 138 GHz Test Series

Resonator. Fabry-Pérot reflection-type, semi-confocal arrangement, 10 cm mirror diameter, 20 cm spacing; micrometer tuning: 0.3175 mm/turn with 1.3×10^{-6} mm resolution; loaded Q value at f_R = 138.2 GHz: Q = 437,000; effective path length (Eq.20): L_R = 0.151 km; Fresnel number: 6; response time constant: $Q/\pi f_R$ = 1.01μs; coupling coefficient: 0.053; coupling hole: circular, 0.65 mm diameter, 0.075 mm double Mylar vacuum/pressure seal.

Excitation. Linearily frequency-modulated klystron with stabilized center frequency; sweep rate: 50 Hz, sweep width 7 MHz or 19600 μs; reflected signal off-resonance: 150 mV.

Detection. Unbiased Schottky diode (β = 2) with precision attenuator for dB-calibration; resonance signal peak sensitivity (Eq.22): ± 0.05 dB/km; accuracy: better than ± 10 percent for α>1 dB/km.

Data Run. An example of measuring water vapor attenuation α_w by detecting the resonance peak signal a_1(Pk) with reference to vacuum (a_o) is shown in Figure 5. Relative humidity was increased from RH = 90 to 100 percent over a two-hour period by raising the water temperature from 6.8 to 8.4°C. Condensing water vapor added several tenths of a degree to the cell temperature; however, at 11°C the mirrors remained free of condensation. Some of the data scatter was caused by drift effects of the spectrometer. The calibration of a_1 with AT (see Figure 4) determines the dB-scale and is completed by a measurement of the Q value via the bandwidth of the resonance.

Results and Discussion

Experimental Results

Pressure scans of the attenuation rate α_w due to H_2O absorption were made at the frequency f_1 = 138.2 GHz. First, pure water vapor pressure e was increased to a constant relative humidity RH, adjusted for values between 80 and 100 percent. Then nitrogen was injected to simulate moist air, although N_2 broadens water vapor lines 1.094

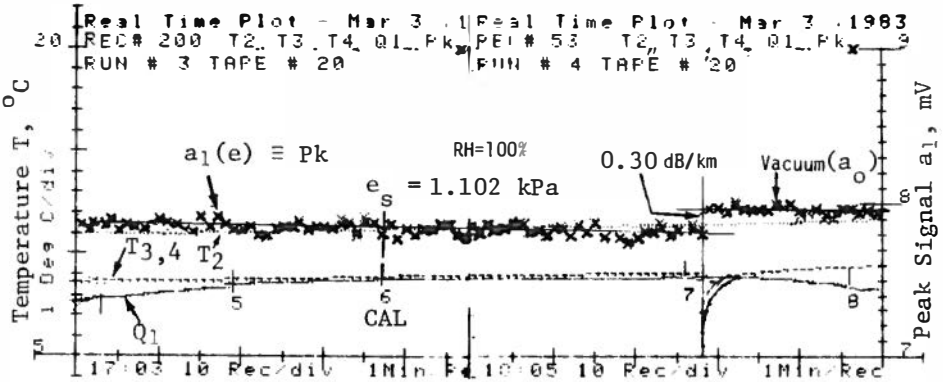

Figure 5. Example of a time series data plot from five instruments, reading temperature: T_2 = mirror, $T_{3,4}$ = cell center and bottom, Q_1 = water; and peak signal Pk (water vapor absorption). The sequence covers a two-hour period during which water vapor saturation was achieved by equalizing the temperature of 8.4°C between cell ($T_{3,4}$) and water (Q_1). CAL = calibration points for a_1 (dB), BW (ms), reference power, and micrometer setting.

more effectively than dry air (15). The test frequency f_1 falls into an EHF window where little attenuation by local lines is expected (see Eq.27). A summary of reduced and calibrated data is shown in Figure 6. A data fit to Eq.(13) at 300 K amounted to

$$\alpha_w = 0.197e^2 + 0.00750ep \quad \text{dB/km}, \tag{24}$$

resulting in

$$m^x = 26.3 = 5.5m \quad . \tag{25}$$

The broadening efficiency m^x is determined by pressure pairs e_1 and P_1--points where water vapor attenuation ($\propto e^2$) and moist nitrogen attenuation [$\propto P(e-1)$] are equal, i.e.

$$m^x = (P_1/e_1) - 1$$

Attenuation at points A (2.40 dB/km, e = 3.49 kPa) and B (5.10 dB/km, P = 106.7 kPa) was studied with special care. Point A was stable over a 40-hour period and independent of the water valve position (open/closed), provided a

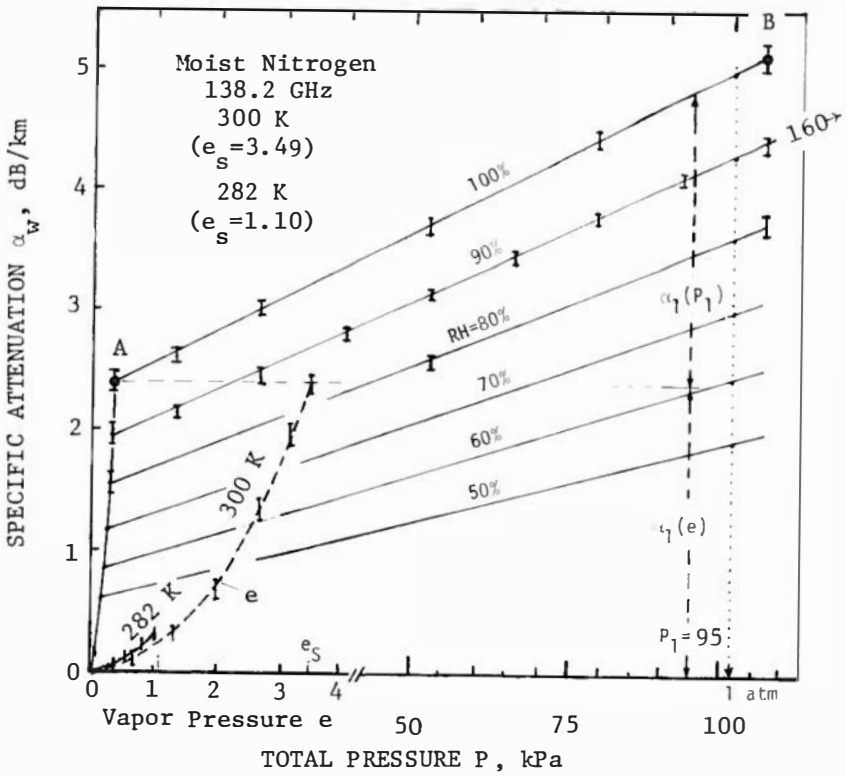

Figure 6. Pressure dependence of specific attenuation α due to water vapor (e) and moist nitrogen (P) measured at 138.2 GHz and relative humidities from RH = 80 to 100 percent.

slight mirror heating (1W) was applied. Increasing the mirror heating to 5W (+4°C) did not change the result. Strong anomalies (condensation effects), on the other hand, were observed when the mirror heaters were off. At point B a very long mixing time (several hours) has to be allowed when the water valve is opened against 110 kPa nitrogen. Faster mixing occurs when nitrogen is blended with water vapor already filling the cell.

Temperature dependence is another diagnostic which can be used to support the theoretical interpretation of continuum attenuation in terms of molecular H_2O line broadening. A series of pure water vapor pressure scans

was made at T = 282 K (see Figure 5). Temperature limited the saturation pressure to 1.102 kPa. A preliminary fit of these data yields (compare with Eq.15)

$$y = 3.5 \pm 1 \qquad (26)$$

Pressure dependence indicated by Eq.(13) has been observed in earlier laboratory (10 to 17, 23, 24) and field (4d, 4e) experiments. A selected review of laboratory data is given in Table IV. The following approximate relations can be deduced from this data body:

$$\alpha_w \simeq k_s(e^2 + ep/m^x) \quad \text{(in between lines);}$$

$$k_s \propto f^2 \quad \text{(excluding the 67.7 GHz data);}$$

$$m^x \propto 1/f^{0.5} \quad \text{(see Ref. 10);}$$

$$y \simeq 5.5 \quad \text{(for the 110 GHz data).}$$

Table IV. Laboratory results for water vapor attenuation α_w fitted to Eq.(13) yielding the coefficient k_s^x and broadening efficiency m^x.

f	k_s^x	m^x	Broadening Agent	T	Ref.
GHz	dB/(km kPa^2)			K	
31	0.011	49*	Air	318	11
67.7	0.16	44*	Air	283	24
110	0.12	35*	Air	304	24
110	0.16	35*	Air	292	23
110	0.21	35*	Air	274	24
138	0.197	26.3(29)	N_2(Air)	300	this
138	0.25	-	-	282	paper
213	0.62	24*	N_2	320	4g, 17
345	2.4 ± 1.5	24	N_2	300	19
411	2.9 ± 0.8	18	N_2	300	19
667	4.1 ± 1.1	9.6	N_2	300	19
883	5.2 ± 1.4	9.4 ± 0.9	N_2	300	19

* Our fit to reported raw data

Absolute data on α_w are difficult to obtain. In spite of existing inconsistencies, our data lend support to the hypothesis that far-wings of self-broadened H_2O lines centered above 1 THz are probably the major source for the EHF continuum (10). Line shape theory needs to be revised to account for the minute ($< 10^{-5}$ the value at line center) contributions in the extreme low frequency wings of pressure-broadened lines located above 1 THz in the rotational H_2O spectrum (4b, 4h, 9, 21, 22).

Water Vapor Continuum and EHF Propagation Modeling

The experimental result at 138.2 GHz for moist nitrogen attenuation (Eq.24) has been incorporated into the EHF propagation model that is based upon LB5 (1,25). Reducing the ep-term by 9.4 percent for air-broadening and subtracting line contributions due to LB5,

$$\alpha_\ell(\text{LB5}) = 1.94 \times 10^{-3}\ \text{ep} + 0.0093\ e^2 \quad \text{dB/km}, \qquad (27)$$

gives the pressure dependence of continuum attenuation as

$$\alpha_c = \alpha_w - \alpha_\ell = 4.86 \times 10^{-3}\ \text{ep} + 0.188e^2 \quad \text{dB/km}. \qquad (28)$$

Adding frequency and temperature dependences to Eq.28 leads to a moist air continuum spectrum for LB5, modeled by

$$N''_c = (c_1 \text{ep}\theta^y + c_2 e^2 \theta^{y^*}) f \times 10^{-6} \quad \text{ppm}. \qquad (29)$$

The coefficients for Eq.(29) are chosen according to the following scheme:

	c_1	y	c_2	y*	Remark
Old	1.90	3.1	0	1	Gaut-Reifenstein
New	1.40	2.5	54.1	3.5	Eqs.28, 15, 26

The "new" continuum spectrum is different from various other empirical forms (summarized in Table V) which have been proposed.

Table VI compares the implications of the old and the new continuum for the case of predicting zenith attenuation A(dB) through a model atmosphere.

Table V. Experimental water vapor continuum coefficients (Eq.6) reported by other workers (2).

k	x(v)	y(T)	u(f)	Local Lines	f, GHz	Ref.
0.023	1.00	2.1	2.50	MVW	50 to 500	10
0.039	1.05	3.0	2.40	GR	20 to 350	18
0.049	1.00	2.1	2.00	VW	15 to 500	(*)
0.061	1.00	2.1	1.22	GR	150 to 410	21

(*) Gaut-Reifenstein model (1).

Table VI. Comparison of zenith attenuation A(dB) predicted for a synthetic atmosphere (30°N, July) by employing the EHF Propagation Model (1,25) with old (Gaut-Reinfenstein) and new (Eq.29) water vapor continuum formulations.

Ray Path Angle: 0.00 Degrees from Zenith

Integrated through Model Atmosphere: p_o = 101.35 kPa, T_o = 301.15 K, 31 Height Levels, h = 0 to 30 km,

Integrated Water Vapor V = 52.69 70.25 mm,

Electric Path Length L_E = 2627.2 2739.0 mm.

FREQUENCY(GHz)	ATTENUATION(dB)		ATTENUATION(dB)	
30.00	.59	.64	.72	.88
35.00	.63	.70	.74	.96
40.00	.79	.90	.91	1.21
45.00	1.13	1.26	1.27	1.64
50.00	2.13	2.29	2.29	2.76
55.00	28.16	28.35	28.36	28.92
60.00	148.98	149.21	149.09	149.75
65.00	23.87	24.14	24.16	24.94
70.00	3.19	3.51	3.49	4.39
75.00	2.42	2.78	2.75	3.78
80.00	2.36	2.77	2.72	3.91
85.00	2.48	2.95	2.89	4.22
90.00	2.69	3.20	3.14	4.63
95.00	2.94	3.52	3.44	5.11
100.00	3.23	3.87	3.79	5.64
105.00	3.58	4.29	4.20	6.24
110.00	4.07	4.84	4.75	6.99
115.00	5.47	6.31	6.23	8.67
120.00	11.89	12.81	12.73	15.39
125.00	5.38	6.39	6.31	9.19
130.00	5.51	6.59	6.52	9.64
135.00	5.92	7.09	7.03	10.40
140.00	6.43	7.68	7.66	11.28
145.00	7.03	8.37	8.41	12.29
150.00	7.75	9.19	9.32	13.47
	old	new	old	new

Summary

Absolute attenuation rates α_w have been measured in the laboratory for pure water vapor and for mixtures of vapor and nitrogen, simulating moist air. Initial studies were performed at 138 GHz, two temperatures (282 and 300 K), partial vapor pressures up to saturation (1.10 and 3.48 kPa), and total pressures up to 160 kPa. Preliminary results were acquired for pressure and temperature dependences of α_w. The data behaved in a fashion similar to that expected from H_2O line-broadening theory (Eq.13). Except for a strong self-broadening component ($\propto e^2$), no additional anomalous behavior was observed--even at saturation pressures (RH = 100%)--contrary to findings by other workers (4,17, etc.).

In our case, we could clearly identify anomalous absorption behavior (e.g., unusually high rates, extreme temperature dependences, hystereses in pressure and temperature cycles) as being instrumental, that is condensation effects on the millimeter wave-active parts of the spectrometer. Considerable effort had to be expended before the instrument produced consistent, reproducible results.

A water vapor continuum N''_c was formulated for the EHF propagation model (1,25) in order to supplement contributions from 30 H_2O lines below 1 THz. At 138 GHz, the local lines furnish 40 percent to air-broadening but only 5 percent to self-broadening of the water vapor attenuation α_w. Practical implications of the continuum to propagation modeling are not too serious. Up to humidities of $v \lesssim 10$ g/m^3, the widely used empirical Gaut-Reifenstein continuum (1) is roughly confirmed. At higher values, increases over the GR continuum and a nonlinear dependence on absolute humidity are predicted.

Acknowledgments

The paper is a revised version of a presentation made at the URSI Com. F 1983 Symposium (26). The author wishes to thank K. C. Allen for programming the line shape models, D. H. Layton for designing the data acquisition system, and V. Wolfe for assisting with the measurements and data evaluation.

References

1. H. J. Liebe, Radio Sci., 16(6), 1183-1199 (1981).

2. H. J. Liebe, IEEE Trans. Ant. Prop., AP-31(1), 127-135 (1983).

3. URSI Commission, URSI Working Party Report, Radio Sci. 16(5), 825-829 (1981).

4. A. Deepak et al. (Eds.) Atmospheric Water Vapor, 1980 Academic Press, New York. Papers by:
   a) D. E. Burch and D. A. Gryvnak, 77-100;
   b) R. J. Nordstrom and M. E. Thomas, 101-112;
   c) H. A. Gebbie, 122-142;
   d) H. J. Liebe, 143-202;
   e) D. C. Hogg, 219-228;
   f) R. A. Bohlander et al., 241-254;
   g) D. T. Llewellyn-Jones, 255-264;
   h) S. A. Clough et al., 25-46.

5. L. S. Rothman, R. R. Gamache, A. Barbe, A. Goldman, J. R. Gillis, L. R. Brown, R. A. Toth, J. -M. Flaud, and C. Camy-Peyret, Appl. Opt. 22(12), 2247-2256 (1983).

6. J. M. Flaud, C. Camy-Peyret, and R. A. Toth, Water Vapor Line Parameters from Microwave to Medium Infrared, Pergamon Press, Oxford, England (1981).

7. M. Mizushima, Int. J. Infrar. Millimeter Waves, 3(3), 379-384 (1982).

8. R. L. Poynter and H. M. Pickett, JPL Publication 80-28, Rev. 1, Jet Propulsion Lab., NASA, Pasadena, CA (1981).

9. M. E. Thomas and R. J. Nordstrom, J. Quant. Spectrosc. Radiat. Trans., 28(2), 81-112 (1982).

10. D. E. Burch, Ford Aerospace and Communications Corp., Aeronutronic Div., Final Report AFGS-TR-81-0300 (March 1982).

11. G. E. Becker and S. H. Autler, Phys. Rev. 70, 300-307 (1946).

12. L. Frenkel and D. Woods, Proc. IEEE 54, 498-505 (1966).

13. C. O. Hemmi and A. W. Straiton, Radio Sci. 4, 9-15 (1969).

14. D. Mrowinski, Z. Angew. Phys. 29, 323-330 (1970) and Ph.D. Thesis 1969, D83 TU, Berlin.

15. H. J. Liebe and T. A. Dillon, J. Chem. Phys. 50(2), 727-732 (1969).

16. H. J. Liebe, OT Report 75-65, (NTIS Acces. No. COM 75-10096/AS) (June 1975).

17. D. T. Llewellyn-Jones, R. J. Knight and H. A. Gebbie, Nature 274(5674), 876-878 (1978).

18. A. Y. Zrazhevskiy, Radio Eng. & Electr. Phys. 21(5), 31-36 (1976) and 22(1), 128-129 (1977).

19. K. A. Aganbekjan and A. Y. Zrazhevskiy, A study of submm. radiation absorption in pure water vapor and in mixtures with N_2, CO_2 and Ar, Private Communication (1982).

20. R. J. Hill, R. S. Lawrence and J. T. Priestley, Radio Sci., 17(5), 1251-1257 (1982).

21. C. C. Zammit and P. A. Ade, Nature 293(5833), 550-552 (1981); and C. C. Zammit, R. E. Hill and R. W. Baker, Int. J. Infrar. Millimeter Waves, 3(2), 189-203 (1982).

22. G. Birnbaum, J. Quant. Spectr. Radiat. Transf. 21, 597-607 (1979).

23. D. T. Llewellyn-Jones and R. J. Knight, IEEE Conf. Publ. 195, 81-83 (1981).

24. R. J. Knight and D. T. Llewellyn-Jones, Rutherford Appleton Laboratory Research Note RL-82-051 (July 1982).

25. H. J. Liebe, A physically-based mm wave propagation model, NTIA Report, to be published.

26. H. J. Liebe and D. H. Layton, Proc. URSI Com. F 1983 Symp., Louvain-La-Neuve, Belgium (ESA SP-194).